Short Papers

Near-Field Absorption Characteristics of Biological Models in the Resonance Frequency Range

MAGDY F. ISKANDER, SENIOR MEMBER, IEEE, STEVEN C. OLSON, AND J. F MCCALMONT

Abstract — **In this paper, we utilized the new iterative extended boundary condition method (IEBCM) to calculate the near-field absorption characteristics of a spheroidal model of man in the resonance frequency range. These calculations complement our previous near-field results in the preresonance frequency range. Calculations were made for simple sources such as an electric dipole and a small current loop antenna. The near fields of these sources are known exactly and hence helped in explaining the absorption results in terms of the field components of the incident radiation. Numerical results for the normalized average SAR values are presented as a function of frequency for different near-field separation distances from the sources. It is generally observed that while the far-field results converge to the plane wave values, different near-field absorption characteristics occur for the two different sources. It was possible in both cases to explain the differences in the near-field average SAR values in terms of the incident near fields from the sources.**

I. Introduction

Among the remaining areas where more work is still needed in RF dosimetry research is the quantification of the near-field absorption by biological models. The near fields are in many cases significantly different from the far field. For example, they are generally characterized by the presence of strongly reactive field components which may also vary rapidly in space. The electric and magnetic field vectors in the near zone are not necessarily orthogonal to each other; nor is the E/H wave impedance ratio equal to the far-field constant impedance value. Since many exposure situations that occur in industrial, medical, and military sites occur in the near- rather than the far-zone fields, there is a growing concern of the possible biological hazardous effects of the near-field radiation and there is a significant need to determine the absorption characteristics of the near fields. It is generally feared that the near fields may possibly contribute to excessively hazardous absorption conditions. In some previous work, near-field SAR calculations for spheroidal models of humans and animals at lower frequencies have been made [1], [2]. Simple sources such as electric and magnetic dipoles and small-aperture sources were used because their near fields are known exactly and this helped in identifying the physical nature of their interaction with the biological models. Even when using more realistic sources such as a large-aperture antenna, the near fields were expanded in terms of the spherical harmonics to facilitate better quantification of the near fields [3]. In all cases, however, the extended boundary condition method (EBCM) was used to solve the integral equation describing the internal fields. Because of the inherent limitations of the EBCM, which basically arise from the process of fitting a single spherical expansion to highly nonspherical biological models, our near-field results were limited to low-frequency calculations. Other near-field absorption calculations in a block model of man were published in [4]. These calculations, although providing the very useful SAR distribution results, suffer from some limitations on the block model solution procedure, as described elsewhere [5].

With the advent of the iterative extended boundary condition method (IEBCM) [6], [7], the instability problem of the EBCM that often resulted in an ill-conditioned system of equations has been overcome. For example, for the spheroidal model of man, the EBCM provided results up to about 50 MHz, while the IEBCM has been used to make absorption calculations up to about 300 MHz, which is over four times the resonance frequency for the model. The main feature which helped overcome the EBCM convergency problem is related to the utilization of several subregional expansions in the IEBCM, as described elsewhere [6]–[9]. The iterative nature of the IEBCM solution helped only in the numerical implementation of the multiple subregional expansions in the solution of the formulated integral equation.

In this paper, the near-field irradiation of prolate spheroidal models by short electric dipoles and small current loop antennas at frequencies up to and beyond resonance will be described. These higher frequency results are obtained by implementing the IEBCM.

The obtained average SAR results will be presented in normalized form with respect to their plane-wave (far-field) values to emphasize the differences between the far- and near-field absorption characteristics. Attempts will also be made to describe the obtained variations in the SAR values in terms of the orientation of the various field components at the surface of the object. Other comparisons between SAR distributions in the far and near fields, particularly at and beyond the resonance frequencies, will also be made.

II. Calculation Procedure

Consider a spheroidal model of an average man which is oriented along the z axis as shown in Fig. 1. The parameters a and b are the semimajor and semiminor axes of the spheroid, respectively, and ϵ^* is the complex permittivity. The near-field source of moment $\bar{P}$ is arbitrarily located at (r, θ, ϕ) as shown in Fig. 1, where r should be larger than the dimension of the major axis of the spheroid (a) to maintain the near-field source outside a spherical region surrounding the object. The absorption problem is first formulated in terms of an integral equation which utilizes the transverse dyadic Green's function [10]. The EBCM or IEBCM solution procedure here involves expanding the known incident and unknown internal fields in terms of vector spherical harmonics and applying the orthogonality property of these functions to determine the unknown expansion coefficients. Therefore, in the near-field calculations, the incident fields from an electrically short electric dipole and from a small current loop antenna were expanded in vector spherical harmonics [10]–[12].

Manuscript received November 1, 1986; revised March 28, 1987

M. F Iskander and J. F. McCalmont are with the Department of Electrical Engineering, University of Utah, Salt Lake City, 84112

S. C. Olson was with the Department of Electrical Engineering, University of Utah. He is now with the Radar System Group, Hughes Aircraft Co., El Segundo, CA.

IEEE Log Number 8715140.

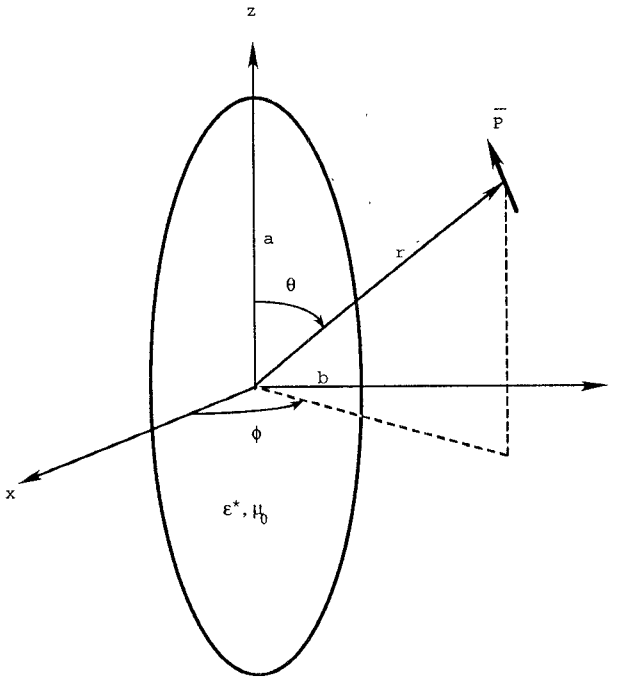

Fig. 1. Geometry of a spherical model irradiated by a near-field source of moment $\bar{P}$ located at (r, θ, ϕ).

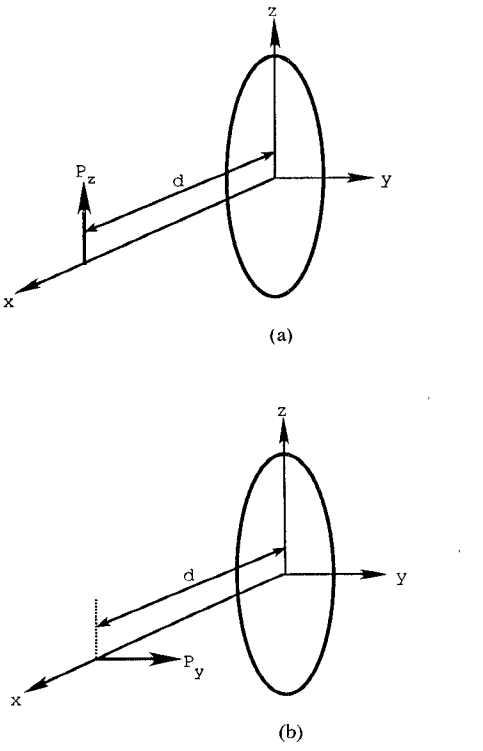

Fig. 2 Location and orientation of the dipole moment of (a) an electrically short electric dipole and (b) a small magnetic dipole (small current loop)

Explicit expressions for the spherical harmonic expansions of the incident fields from an electrically short electric dipole of moment $\bar{P}$ and from a small current loop of a magnetic moment $\bar{m}$ are given elsewhere [12], [13], [1], [16]. The unknown coefficients included in the expansions of the internal fields, on the other hand, were determined iteratively using the IEBCM procedure described elsewhere also [6].

III. Numerical Results

Numerical calculations were made for the specific cases where the electric and magnetic dipoles were oriented so as to correspond to the E-polarization case for the plane-wave exposure, which is the orientation that causes maximum absorption in the resonance frequency range. Specifically, for the electric dipole case, the dipole was located at $\phi = 0°$ and $\theta = 90°$, with the dipole moment oriented along the z direction as shown in Fig. 2(a). For the small current loop case, it is also located at $\phi = 0°$ and $\theta = 90°$ except that the magnetic dipole moment is oriented along the y direction as shown in Fig. 2(b).

To verify the accuracy of the numerical procedure, comparison was made between the specific absorption rate (SAR) axial distribution in a spheroidal model of an average man ($a = 0.875$, and $a/b = 6.34$) when irradiated by the fields of a dipole located at large separation distance $d = 2\lambda$ from the center of the spheroid and when exposed to the plane-wave-radiation, E-polarization case. These SAR distribution values are given in Table I for both the electric and magnetic dipole cases at different frequencies. It is clear that the results from both cases are in good agreement. The complex permittivity was taken equal to 2/3 that of the muscle tissue; e.g., $\epsilon' = 78.5$ and $\epsilon'' = 270$ at 27 MHz and $\epsilon' = 43$ and $\epsilon'' = 112$ at 100 MHz [14]. Furthermore, the magnitude of the dipole moment $\bar{P}$ (P_z for the electric and P_y for the magnetic dipole cases) is normalized so that the average SAR's obtained for a dipole located at a large distance (2λ) from the spheroid are equal to those values obtained from the plane-wave exposure. Since the far-field radiated power (time-average Poynting vector) from the dipole is inversely proportional to the square of the distance from the spheroid [15], it is necessary to adjust the value of the normalization constant accordingly so as to obtain SAR values that correspond to the same value of the incident time-average power associated with the incident radiation. Therefore, any differences in the near-field SAR values are due to factors different from those due to the $1/r^2$ incident far-field power density variation [1].

A. Numerical Results for the Electric Dipole Case

For the electric dipole case the average SAR values as a function of frequency for three different separation distances (d) from the source are shown in Fig. 3. From Fig. 3 it is clear that all the SAR values of these specific distances from the source tend to converge to the plane-wave value at higher frequencies where d/λ approaches 2. It is also clear that the near-field average SAR values in the resonance frequency range (values of d/λ in the frequency band range from $0.20 \leqslant d/\lambda \leqslant 0.58$) are smaller than the plane-wave average SAR's. This can be explained in terms of the variation in the relative magnitudes of the various components of the electric fields incident from the electric dipole. At large distances ($d/\lambda > 1.0$) the incident electric field is dominated by a component parallel to the major axis of the spheroid. This field component is strongly coupled to the dielectric spheroid since it is tangential to the major part of its elongated surface along the major axis. Examination of incident electric field components from the electric dipole at smaller separation distances [2] (i.e., $0.1 < d/\lambda < 1.0$) also showed that the component of the field normal to the surface of the spheroid starts to dominate as the electrical distance decreases from $d/\lambda = 0.5$ to $d/\lambda = 0.1$. According to the electric field boundary conditions at the surface of the spheroid, this dominant electric field component is weakly coupled to the dielectric spheroid [2] and hence causes the reduction in the average SAR value for the

TABLE I
COMPARISON BETWEEN THE FAR-FIELD SAR VALUES FOR ELECTRIC AND MAGNETIC DIPOLE SOURCES AND THOSE OBTAINED FROM THE PLANE-WAVE INCIDENT RADIATION CASE

(Axial) Point Location (r,θ,φ)	SAR (W/Kg)								
	27 MHz			73 MHz			100 MHz		
	Electric Dipole d/λ =2.0	Magnetic Dipole d/λ =2.0	Plane Wave	Electric Dipole d/λ =2.0	Magnetic Dipole d/λ =2.0	Plane Wave	Electric Dipole d/λ =2.0	Magnetic Dipole d/λ =2.0	Plane Wave
(a,0,0)	.00152	.00152	.00150	.01630	.01640	.01610	.00692	.00690	.00644
(3/4 a,0,0)	.00156	.00156	.00154	.02340	.02360	.02320	.00900	.00900	.00868
(a/2,0,0)	.00161	.00161	.00160	.02940	.02960	.02920	.01230	.01230	.01220
(a/4,0,0)	.00166	.00167	.00165	.03310	.03350	.03300	.01400	.01410	.01410

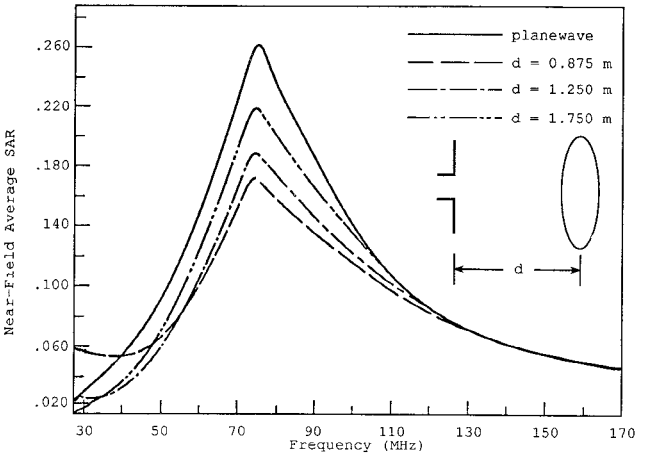

Fig. 3 Normalized (with respect to plane-wave values) average near-field SAR's in a spheroidal model of an average man ($a = 0.875$ m, $a/b = 6.34$) as a function of frequency. The near-field source is an electric dipole oriented parallel to the major axis of the spheroid

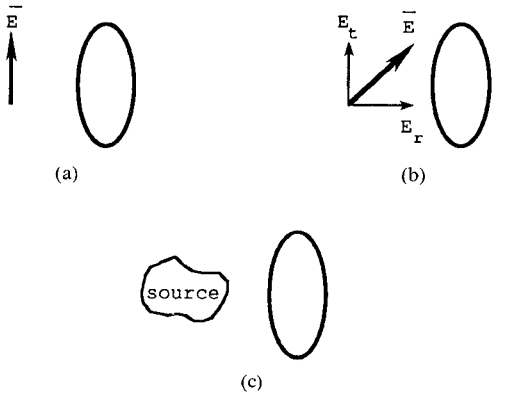

Fig. 4 Source-to-object coupling characteristics for the case of an electric dipole source radiating in the presence of a biological model of man (a) Far field is strongly coupled and there are large values of the average SAR. (b) Near field ($0.2\lambda < d < 0.5\lambda$) with E_r weakly coupled and E_t strongly coupled; the final result is a reduction in average SAR. (c) Near field ($d < 0.1\lambda$) with complicated strong coupling, where mutual interaction should be taken into account.

same incident power. Finally, for $d/\lambda < 0.1$ (i.e., at frequencies of about 34 MHz for the specific distances given in Fig. 3), we note an increase in the average SAR values. This is particularly clear for the smallest chosen value of $d = 0.875$ m, where the electrical distance d/λ starts getting smaller than 0.1 at 34.3 MHz. This noted increase in the average SAR may be due to the strong coupling between the source and the spheroid and to the major role played by the reactive energy stored near the source. It should be emphasized, however, that the results obtained in this very close proximity from the source are only a zeroth-order approximation, since modification of the incident fields from the source as a result of the interaction between the source and the object should be taken into account at these small separations. This mutual interaction has not been taken into account in this paper and further refinement in the average SAR values is needed, therefore. Fig. 4 summarizes the source-to-object coupling effects found in studying the interaction of the short electric dipole with a spheroidal model of man at three distinct separation-distance ranges.

B. Numerical Results for the Magnetic Dipole Case

For the small current loop antenna case, Fig. 5 shows comparison of the variation of the average SAR versus frequency for a plane-wave case and for a y-directed magnetic dipole (see Fig. 2(b)) located at three specific distances from the source: $d = 0.875$, $d = 1.250$, and $d = 1.750$ m. As in the case of the electric dipole, the SAR values corresponding to these distances from the source also converge to the plane-wave values at the higher frequencies ($f > 100$ MHz) where the electrical distance d/λ becomes larger than approximately 0.5. However, the near-field SAR characteristics of the loop antenna are quite different from those of the electric dipole in the frequency band from 27 MHz to about 100 MHz. As the electric separation distance (d/λ) decreases, it is seen from Fig. 5 that the near-field average SAR's are higher than the corresponding plane-wave values in the same frequency range. These near-field characteristics can also be explained in terms of the orientation and magnitude of the incident electric and magnetic field components of the current loop [16] with respect to the spheroidal model. From the incident field calculations [17], it was found that in addition to the electric and magnetic field components which are oriented in directions similar to those associated with the plane-wave E-polarization case, there is another magnetic field component, H_r, which increases in magnitude with the decrease of the separation distance from the source. In other words, as d/λ decreases, a radial magnetic field component whose magnitude was negligible at larger values

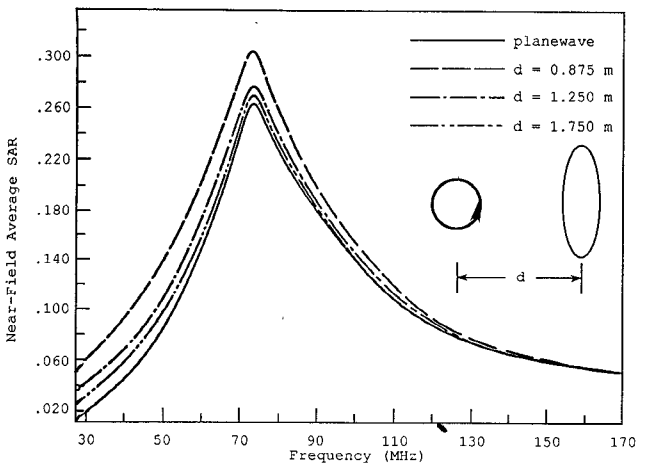

Fig. 5. Normalized values of the near-field average SAR's in a spheroidal model of an average man ($a = 0.875$ m, $a/b = 6.34$) as a function of frequency. The near-field source is a magnetic dipole (small current loop antenna) oriented so that the far electric field is parallel to the major axis of the spheroid.

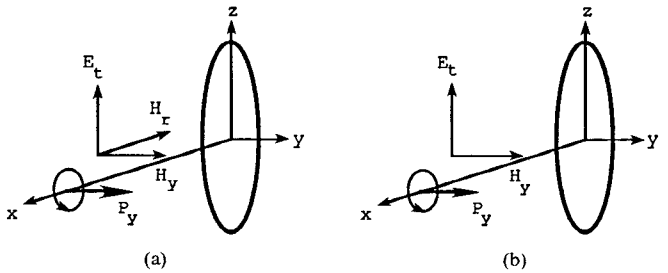

Fig. 6. Source-to-object near-field coupling for a magnetic dipole source. (a) Near field, where the additional H_r introduces stronger coupling and, hence, a further increase in the average SAR values. (b) Far field, where there is strong $\bar{E}$ and $\bar{H}$ field coupling and large average SAR values.

of d/λ begins to increase in the near-field region. It is shown elsewhere [2] that this magnetic field component is strongly coupled to the spheroid, and hence causes an increase in the absorption, since it is oriented perpendicular to the major axis of the spheroid. It should be noted that for smaller separation distance ($d = 0.875$), a more significant increase in the average SAR is observed. This, once again, may be explained in terms of the increase of H_r with the decrease of the electrical distance from the source. A summary of the coupling between the magnetic dipole and the dielectric object is shown in Fig. 6.

IV. Discussion of Near-Field Results

Near-field SAR values were calculated up to and beyond the resonance frequency range of a prolate spheroidal model of an average man. These new calculations were made possible with the advent of the IEBCM, which overcomes the convergence problems of the EBCM. The near-field absorption of the prolate spheroidal model was evaluated by using two sources, a short electric dipole and a small current loop (magnetic dipole) antenna.

The orientation of the sources was such that the average SAR from each source could be compared with the corresponding E-polarized plane-wave values. The absorption characteristics due to both sources were found to be quite different except at larger separation distances ($d/\lambda > 0.5$), where they both converge to the plane-wave values. Also, for both sources, as the source-to-object distance decreases, the interaction of the object with the source should be taken into account. Because we neglected such an iteration we did not report SAR's at distances smaller than 0.1λ.

In order to obtain meaningful results, the SAR results were normalized with respect to the plane-wave value at each frequency. The normalization was performed so as to separate the absorption characteristics due to the near fields (i.e., not due to the monotonic $1/r^2$ increase in SAR as the object approaches the source). Hence, our normalization procedure is based on keeping the time-average Poynting vector the same at all separation distances from the source. The time-average Poynting vector is related to the power supplied to the antenna (dipole) and the distance from the source at which the power density is being measured. With such a normalization procedure, any new absorption characteristics should be attributed to detailed near-electric-field and near-magnetic-field interactions with the object.

In summary, the calculated SAR results in the resonance range conform with the understanding previously obtained from the plane-wave and low-frequency near-field exposure case. In particular, it is emphasized that meaningful evaluation of hazardous levels of RF radiation should be made in terms of the magnitudes and directions of the incident electric and magnetic field components, rather than the incident power density level. These near-field exposure findings are certainly important for implementation in the process of developing adequate safety standards for RF exposures and also in designing RF personnel dosimeters which alert workers to the presence of hazardous levels of radiation. It is important to note that we have evaluated the interaction between a dielectric object and two simple sources (electric and magnitude dipole), each having known fields to help us better quantify near-field dosimetry and better understand the physical nature of the interaction. The developed understanding, however, may be applied to more complicated near-field sources.

References

[1] M. F. Iskander, P. W. Barber, C. H. Durney, and Durney, and H. Massoudi, "Irradiation of prolate spheroidal models of humans and animals in the near-field of a short electric dipole," *IEEE Trans. Microwave Theory Tech.*, vol. MTT-28, pp. 801–807, 1980.

[2] M. F. Iskander, H. Massoudi, C. H. Durney, and S. J. Allen, "Measurements of the RF power absorption in spheroidal human and animal phantoms exposed to the near-field of a dipole source," *IEEE Trans. Biomed. Eng.*, vol. BME-28, pp. 258–264, 1981.

[3] A. Lakhtakia and M. F. Iskander, "Scattering and absorption characteristics of lossy dielectric objects exposed to the near-fields of aperture sources," *IEEE Trans. Antennas Propagat.*, vol. AP-31, pp. 111–120, 1983.

[4] K. Karimulah, K.-M. Chen, and D. P. Nyquist, "Electromagnetic coupling between a thin-wire antenna and a neighboring biological body: Theory and experiment," *IEEE Trans. Microwave Theory Tech*, vol. MTT-28, pp. 1218–1225, 1980.

[5] H. Massoudi, C. H. Durney, and M. F. Iskander, "Limitations of the cubical block model of man in calculating SAR distribution," *IEEE Trans. Microwave Theory Tech.*, vol. MTT-32, pp. 746–752, 1984.

[6] M. F. Iskander, A. Lakhtakia, and C. H. Durney, "A new procedure for improving the solution stability and extending the frequency range of the EBCM," *IEEE Trans. Antennas Propagation.*, vol. AP-31, pp. 317–324, 1983.

[7] A. Lakhtakia, M. F Iskander, and C. H. Durney, "An iterative extended boundary condition method for solving the absorption characteristics of lossy dielectric objects of large aspect ratios," *IEEE Trans. Microwave Theory Tech.*, vol. MTT-31, pp. 640–647, 1983.

[8] A. Lakhtakia and M. F. Iskander, "Theoretical and experimental evaluation of power absorption in elongated biological objects at and beyond resonance," *IEEE Trans. Electromag. Compat.*, vol. EMC-25, pp. 448–453, 1983.

[9] M. F. Iskander and A Lakhtakia, "Extension of the iterative EBCM to calculate scattering by low-loss or lossless elongated dielectric objects," *Appl. Opt.*, vol. 23, pp. 948–952, 1984.

[10] P W. Barber, "Electromagnetic power deposition in prolate spheroidal models of man and animals at resonance," *IEEE Trans. Biomed. Eng.*, vol. BME-24, pp. 513–521, 1977

[11] J. D. Jackson, *Classical Electrodynamics*. New York: Wiley, 1962.

[12] A. Hızal and Y K. Baykal, "Heat potential distribution in an inhomogeneous spherical model of a cranial structure exposed to microwave due to loop or dipole antenna," *IEEE Trans. Microwave Theory Tech*, vol. MTT-26, pp 607–612, 1978.
[13] H. Chew, P J McNutley, and M Kerker, "Model for Raman and fluorescent scattering by molecules embedded in small particles," *Phys. Rev. A*, vol. 13, pp 398–404, 1976
[14] C. H. Durney, P. C Johnson, P. W Barber, H. Massoudi, M. F. Iskander, J. L. Lords, D. K. Ryser, and S. J. Allen, and J. C. Mitchell, *Radiofrequency Radiation Dosimetry Handbook*, 2nd ed. Department of Electrical Engineering, University of Utah, Salt Lake City, 1978.
[15] E. J. Jordan and K. Balmain, *Electromagnetic Waves and Radiating Systems*, 2nd ed. Englewood Cliffs, NJ: Prentice-Hall, 1968
[16] A. Lakhtakia, M. F. Iskander, C. H. Durney, and H. Massoudi, "Near-field absorption in prolate spheroidal models of humans exposed to a small loop antenna of arbitrary orientation," *IEEE Trans. Microwave Theory Tech.*, vol. MTT-29, pp. 588–594, 1981.
[17] L. M. Magid, *Electromagnetic Fields, Energy, and Waves* New York: Wiley, 1972.

AM–AM and AM–PM Measurements Using the PM Null Technique

JAMES F. MOSS, MEMBER, IEEE

Abstract —**This paper describes a new method for measuring AM–AM and AM–PM nonlinearities in microwave radio components. This new method is called the PM null technique. This method is accurate and easy to implement. Both the carrier and modulation frequencies can be changed easily. Results of AM–AM and AM–PM measurements performed on a 8-GHz amplifier are given. This new method was compared with Moffatt's parabolic phase method and found to be in good agreement.**

I. INTRODUCTION

If the gain of a two-port network is dependent on the input amplitude, amplitude modulation to amplitude modulation (AM–AM) conversion will occur. If the phase shift through a two-port network is dependent on the input amplitude, amplitude modulation to phase modulation (AM–PM) conversion will occur. If an AM signal is injected into a two-port network, the AM–AM conversion will change the modulation index. If the network has an AM–PM conversion, the phase of the output signal will be modulated at the same rate as the input AM modulation.

There are several methods of measuring AM–AM and AM–PM conversion [1]–[3]. The method described here, the PM null technique, is the most direct, uses simple components, and is highly accurate.

The PM null technique works as follows: An AM signal with very little residual PM is input to the device under test (DUT). A calibrated AM receiver at the DUT output demodulates the AM component, ignoring the PM sidebands. This baseband output is a measure of the modulation index at the output of the DUT. By comparing the input and the output modulation indices, the AM–AM conversion can be found. Similarly, if the output signal is demodulated by a calibrated PM receiver, the AM sidebands will be ignored, and the baseband output will be proportional to the peak phase deviation. Since the input signal has no PM component, the PM measured must be caused by the DUT nonlinearities. Comparing the input AM modulation index and the output peak phase deviation yields the AM–PM conversion.

Manuscript received September 26, 1986, revised April 6, 1987.
The author is with AT&T Bell Laboratories, North Andover, MA 01845
IEEE Log Number 8715418

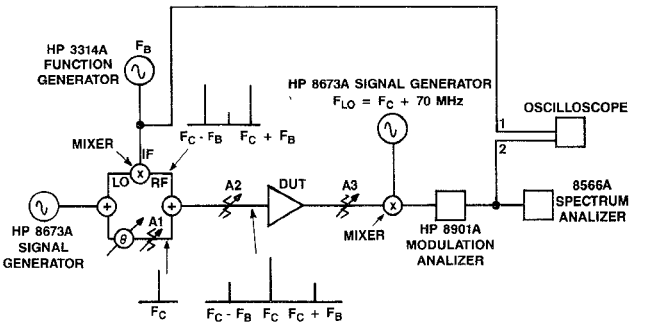

Fig. 1 AM/AM and AM/PM measurement test set

The PM null method requires the following equipment:

1) a PM demodulator with $\leqslant 0.05°$/dB AM–PM and $\geqslant 30$ dB AM suppression;
2) an AM demodulator with > 30 dB PM suppression;
3) an AM modulator with < 0.001 radian peak residual PM;
4) a down-converter with $< 0.05°$/dB AM–PM and < 0.05 dB AM–AM.

An HP 8901A modulation analyzer was used as both the AM and PM demodulator. The 8901A has excellent AM and PM suppression and negligible AM–PM. The modulation frequency must be 100 kHz or less when using the 8901A. If a higher modulation rate is required, a different PM demodulator, such as the 4A FM receiver [4] used by Moffatt, must be used. The down-converter can be made with a commercially available, double-balanced wide-band mixer. The RF input to the mixer is kept backed off from its 1-dB compression point so that the mixer AM–AM and AM–PM will be very small.

The PM null technique requires a modulator with nearly ideal characteristics. Stremler [5] suggests modulators generating AM and narrow-band PM signals. By adding a variable phase shifter of the type shown in Fig. 1, the modulation format can be changed from AM to PM simply by adjusting the phase shifter.

The modulator operation can be explained as follows: A signal at the carrier frequency F_c is split into two arms. One arm contains a phase shifter and an attenuator. The other arm contains a wide-band double-balanced mixer. The mixer up-converts the modulation frequency F_B, producing sidebands at $F_C - F_B$ and $F_C + F_B$. The carrier frequency level at the double-balanced mixer output will be very low compared to the sideband levels because of good local oscillator (LO) suppression. The two arms are recombined at the modulator output. The output spectrum contains a carrier at F_C and sidebands at $F_C - F_B$ and $F_C + F_B$. If the phase shifter is adjusted so that the sidebands are in phase with the carrier, a pure AM signal is generated. If the modulation index is $\ll 1$ and the phase shifter is adjusted such that the sidebands are 90° out of phase with respect to the carrier, a pure narrow-band PM signal is generated. The modulation index can be adjusted with attenuator A1. It is important to maintain the modulation index at 0.1 or less so that the narrow-band approximation is valid.

The phase shifter can be adjusted by demodulating the modulator output in a PM receiver. When the phase shifter is adjusted for a maximum baseband response, a pure PM signal is being generated. If the phase shifter is adjusted for a null or minimum of the baseband response, a pure AM tone is being